Liquid Crystals
Publication details, including instructions for authors and subscription information:
http://www.informaworld.com/smpp/title~content=t713926090

The B_2-B_7 phase transition in symmetrical bent-shaped mesogens with methoxy substitution

Vladimíra Novotná[a]; Věra Hamplová[a]; Miroslav Kašpar[a]; Milada Glogarová[a]; Karel Kníže k[a]; Siegmar Diele[b]; Gerhard Pelzl[b]; Chris Jones[c]; David Coleman[c]; Noel A. Clark[c]
[a] Institute of Physics, Academy of Sciences of the Czech Republic, 182 21 Prague 8, Czech Republic [b] Institut für Physikalische Chemie, Martin-Luther Universität Halle-Wittenberg, Mühlpforte 1, Germany [c] Department of Physics and Ferroelectric Liquid Crystal Material Research Center, University of Colorado, Boulder, USA

To cite this Article Novotná, Vladimíra , Hamplová, Věra , Kašpar, Miroslav , Glogarová, Milada , Knížek, Karel , Diele, Siegmar , Pelzl, Gerhard , Jones, Chris , Coleman, David and Clark, Noel A.(2005) 'The B_2-B_7 phase transition in symmetrical bent-shaped mesogens with methoxy substitution', Liquid Crystals, 32: 8, 967 — 975
To link to this Article: DOI: 10.1080/02678290500284132
URL: http://dx.doi.org/10.1080/02678290500284132

Liquid Crystals, Vol. 32, No. 8, August 2005, 967–975

Taylor & Francis
Taylor & Francis Group

The B_2–B_7 phase transition in symmetrical bent-shaped mesogens with methoxy substitution

VLADIMÍRA NOVOTNÁ*†, VĚRA HAMPLOVÁ†, MIROSLAV KAŠPAR†, MILADA GLOGAROVÁ†, KAREL KNÍŽEK†, SIEGMAR DIELE‡, GERHARD PELZL‡, CHRIS JONES§, DAVID COLEMAN§ and NOEL A. CLARK§

†Institute of Physics, Academy of Sciences of the Czech Republic, Na Slovance 2, 182 21 Prague 8, Czech Republic
‡Institut für Physikalische Chemie, Martin-Luther Universität Halle-Wittenberg, Mühlpforte 1, Germany
§Department of Physics and Ferroelectric Liquid Crystal Material Research Center, University of Colorado, Boulder, CO 80309, USA

(*Received 14 March 2005; accepted 20 May 2005*)

New mesogens composed of achiral bent molecules with thermally stable ester linkages, and laterally substituted by a methoxy group symmetrically near the central benzene ring, were synthesized. Texture, calorimetric, electro-optical, X-ray and dielectric measurements were performed. In most of studied compounds the antiferroelectric B_2 phase was found on cooling from the isotropic phase, followed by the B_7 phase at lower temperatures. Undulation of layers in the B_7 phase was confirmed by precise synchrotron studies.

1. Introduction

Liquid crystals composed of banana-like (bent-core) molecules have become an important subfield in the investigation of mesogenic compounds [1–6]. Chiral polar phases can exist even when the banana-like molecules are non-chiral. Then the bent molecules packed in layers are tilted with respect to the layer normal [2]. Polarization switching originates from ordering of molecular dipoles within smectic layers by an external electric field. Such a phase denoted as the B_2 phase could be regarded as a polar SmC phase and exhibits ferro- or antiferro-electric properties. Among other banana-mesophases the B_7 phase attracts attention due to its unusual character. On the basis of synchrotron X-ray scattering, freeze fracture and optical observations, a model with a commensurable one-dimensional undulation of smectic layers perpendicular to the layer normal has been proposed [7].

First reported materials were Schiff's base resorcinol derivatives, but other linking groups have been used recently, which have a positive effect to the thermal stability of prepared compound [8–18]. The type of substituent connected to either the central or the outer ring may change the dipole moment and influence the formation of mesophases [8]. Moreover, a lateral substituent decreases relatively high phase transition temperatures.

Herein we present a new series based on a 1,3-phenylene unit in the centre with ester linkages and lateral substitution by methoxy groups near the central benzene ring core. The character of the mesophases has been identified using DSC studies, texture observation, electro-optical measurements and high resolution X-ray diffraction.

2. Synthesis

The general formula of the materials studied is shown in scheme 1. Compounds having alkoxy terminal chains (**5WBVI**, **iWBVI**, **8WBVI**) were prepared by an analogous synthetic route as previously described for compound **10WBVI** [19]. Two compounds with alkyl terminal chains (**8WDVI** and **10WDVI**) were synthesized by the general route described in scheme 2.

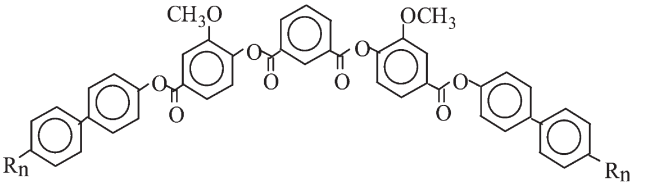

Scheme 1. General formula of compounds studied. R_n designates alkyl or alkoxy chains.

*Corresponding author. Email: novotna@fzu.cz

Liquid Crystals
ISSN 0267-8292 print/ISSN 1366-5855 online © 2005 Taylor & Francis
http://www.tandf.co.uk/journals
DOI: 10.1080/02678290500284132

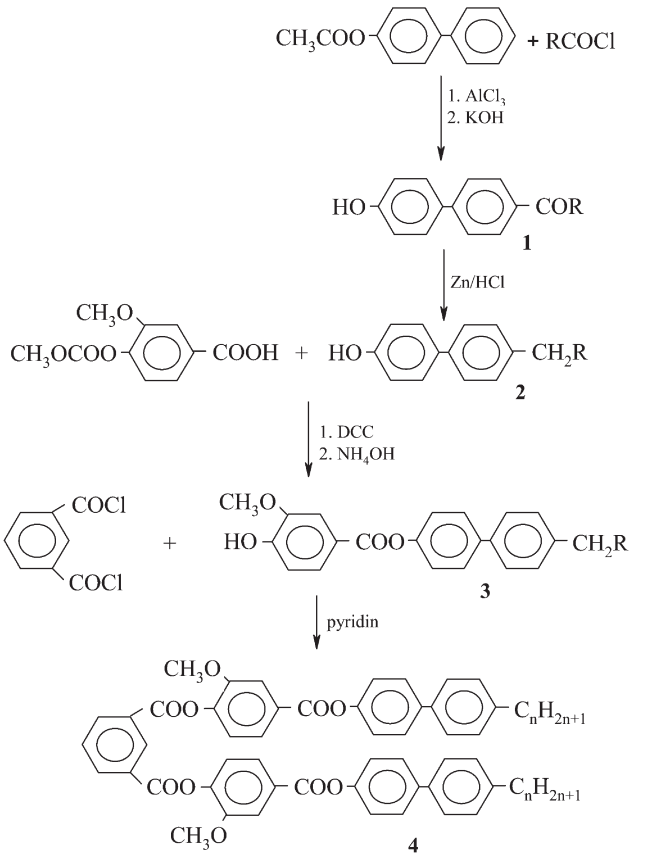

Scheme 2. Synthetic route for the preparation of compounds with alkyl terminal chains.

2.1. *Preparation of 4-(4′-hydroxybiphenyl)alkylketone (1)*

Dry dichloroethane (500 ml), anhydrous aluminium chloride (76 g, 0.52 mol) and 4-acetoxybiphenyl (71 g, 0.33 mol) were stirred under cooling in a water/ice bath and freshly distilled acetylchloride (0.33 mol) was added dropwise during one hour. The reaction mixture was then stirred at room temperature for 8 h and left to stand overnight. After pouring into an ice/HCl mixture, the organic layer was separated, washed with water several times and the solvent removed *in vacuo*. The residue was dissolved in 250 ml of diethyl ether and held at −20°C overnight in a refrigerator. The precipitate was filtered off by suction. The *para*-isomer shows poor solubility in diethyl ether at low temperatures in contrast to the *ortho*-isomer, so this method seems to be very good for separation of the two.

The crude product was dissolved in hot ethanol (300 ml) and a solution of 37 g of potassium hydroxide in water was added dropwise. After cooling, the yellow solution was filtered, poured into 1 l of water and acidified by HCl. The precipitate was filtered off and crystallized from a methanol/dioxan (5/2) mixture. A 55% yield of white crystals was obtaied. ^{1}H NMR (200 MHz, $CDCl_3$) R=C_9H_{19}: 8.05 d, J=8.4 (2H, HAr *ortho* to –CO); 7.55–7.65 m (4H, HAr); 6.95 d, J=8.4 (2H, HAr *ortho* to OH); 3.0 t, J=7.3 (2H, $\underline{CH_2}CO$); 1.8quint (2H, $\underline{CH_2}CH_2CO$); 1.2–1.7 m (12H, CH_2); 0.95 t, J=6.6 (3H, CH_3).

2.2. *Synthesis of 4-alkyl-4′-hydroxybiphenyl (2)*

Granulated amalgamated zinc (150 g) was added to a suspension of 40 g of 4-(4′-hydroxybiphenyl) alkylketon (**1**) in 300 ml of ethanol and 150 ml of concentrated hydrochloric acid. The mixture was reflux heated under with vigorous stirring for 4 days and an additional 100 ml of concentrated HCl added after every 12 h. Residual zinc was removed and the suspension poured over ice. The precipitate formed was collected, washed with water, crystallized from ethanol and dried in vacuum at 60°C. ^{1}H NMR (200 MHz, $CDCl_3$) R=C_9H_{19}: 7.5 m (4H, HAr); 7.23 d, J=8.0 (2H, HAr *ortho* to –CH_2); 6.9 d, J=8.0 (2H, HAr *ortho* to –OH); 2.61 t, J=7.4 (2H, CH_2Ar); 1.6 quint (2H, $\underline{CH_2}CH_2$Ar); 1.2–1.5 m (14H, CH_2); 0.9 t, J=7.0 (3H, CH_3).

2.3. *Preparation of mesogenic phenol (3)*

The mesogenic phenol was prepared by esterification of protected vanillic acid by the appropriate 4-alkyl-4′-hydroxybiphenyl (**2**) in dry dichloromethane. Dicyclohexylcarbodiimide was used as a condensation agent and DMAP as a catalyst. The mixture was stirred for several hours at room temperature; dicyclohexylurea was filtered off and the solvent was evaporated. A 25% solution of NH_4OH in a mixture of chloroform/ethanol (1/1) was used for amonolysis at laboratory temperature. The deprotected product was separated by filtration of the reaction mixture at 0°C. The solid was dissolved in dichloromethane, washed with 10% solution of HCl and water to remove the rest of the ammonia salt, and then evaporated to dryness. Crude product was obtained by crystallization from ethanol and dried *in vacuo*. ^{1}H NMR (200 MHz, $CDCl_3$) R=C_9H_{19}: 7.82 dd, J_1=8.0, J_2=2.1 (1H, HAr *para* to –OCH_3); 7.7d, J=2.0 (1H, HAr *ortho* to –OCH_3); 7.55 m (4H, HAr *ortho* to –Ar); 7.25 m (4H, HAr meta to –Ar); 7.0 d, J=8.0 (1H, HAr *ortho* to –OH); 3.97 s (3H, OCH_3); 2.65 t, J=7.3 (2H, CH_2Ar); 1.1–1.7 m (16H, CH_2); 0.9 t, J=7.0 (3H, CH_3).

2.4. *Preparation of final product (4)*

The final product was obtained by esterification of the mesogenic phenol (**3**) by isophthaloyl dichloride in dichloromethane/pyridine mixture. The reaction

mixture was heated at reflux for several hours; it was cooled, washed with dilute HCl and water and evaporated. The product was crystallized from toluene/acetone and toluene/methanol mixtures and purified by column chromatography on silica gel (Kieselgel 60, Merck, particle size 0.063–0.2 mm) using a mixture of dichloromethane and acetone (99.5/0.5) as eluant.

The chemical purity of the compounds was checked by HPLC, which was carried out with an Ecom HPLC chromatograph using a silica gel column (Separon 7 μm, 3 × 150, Tessek) with a mixture of 99.9% of toluene and 0.1% of methanol as eluant, and detection of the eluting products by a UV-Vis detector (λ=290 nm). The chemical purity was found to be more than 99.9% under these conditions.

2.5. *NMR spectra of final products*

The structures of all intermediates and final products were confirmed by ^{1}H NMR spectroscopy (200 MHz, $CDCl_3$, Varian, Gemini 2000). ^{1}H NMR of the final product **10WDVI**: (200 MHz, $CDCl_3$), R_n=$C_{10}H_{10}$, 9.1 s (1H, between –COO in isophthalic acid); 8.5 d, J=8.0 (2H, *ortho* to –COO in isophthalic acid); 7.9 dd+s (4H, *ortho* and *para* to –OCH_3); 7.75 t, J=8.0 (1H, *meta* to –COO in isoph. acid); 7.6 m (8H, HAr *ortho* to –Ar); 7.3 m (8H+2H, HAr *meta* to –Ar, *meta* to –OCH_3); 3.97 s (6H, OCH_3); 2.65 t, J=7.3 (4H, CH_2Ar); 1.1–1.7 m (32H, CH_2); 0.9 t, J=7.0 (6H, 2 × CH_3).

3. Experimental

Texture observation was performed with a polarizing microscope, Nikon Eclipse E-600. For temperature control a Linkam heating stage was used, which enabled temperature stabilization within ±0.1 K. Studies were carried out on planar samples, usually 6 μm thick. The cells, composed of glass plates provided with ITO electrodes, were filled in the isotropic phase. In several cases commercial Linkam cells (5 μm thick) were used. The birefringence of domains was determined under the microscope with an optical compensator at various wavelengths selected by filters.

Phase transitions were studied by DSC measurements (Perkin–Elmer Pyris Diamond). The samples of about 3 mg were hermetically closed in aluminium pans. Heating and cooling rates of 5 K min^{-1} were applied.

Dielectric properties were studied using a Schlumberger 1260 impedance analyser. The frequency dispersions were measured on cooling at a rate of about 0.2 K min^{-1}, keeping the temperature of the sample stable during frequency sweeps in the range 10 Hz–1 MHz. The frequency dispersion data were analysed using the Cole–Cole formula for the frequency dependent complex permittivity $\varepsilon(f)=\varepsilon'-i\varepsilon''$:

$$\varepsilon^* - \varepsilon_\infty = \frac{\Delta\varepsilon}{1+(if/f_r)^{(1-\alpha)}} - i\frac{\sigma}{2\pi\varepsilon_0 f^n} + Af^m$$

where f_r is the relaxation frequency, $\Delta\varepsilon$ is the dielectric strength, α is the distribution parameter of the relaxation, ε is the permittivity of vacuum, ε_∞ is the high frequency permittivity and n, m, A are fitting parameters. The second and third terms in the equation are used to eliminate a low frequency contribution from d.c. conductivity σ and a high frequency contribution due to the resistance of the ITO electrodes, respectively.

Free-standing films were prepared near the mesophase just below the clearing point by spreading the melted material over a metal slot. The film persisted when heated to the isotropic phase and then cooled. This procedure lowered the number of defects in the film. Spontaneous polarization was investigated using a Sawyer–Tower circuit with compensation of d.c. conductivity and linear capacity. For polarization switching an electrical voltage up to 150 V was applied. A memory oscilloscope, leCroy 9304, provided the switching current profile versus time. An applied triangular electric field from 5 to 60 Hz was used. All materials were studied by X-ray diffraction using the Guiner film method. Experiments were conducted on non-oriented samples in the reflection mode. More precise measurements were performed on the X10A beamline at the National Synchrotron Light Source at Brookhaven for two compounds, **8WBVI** and **10WBVI**. The X-ray wavelength was 1.5481 Å and the resolution was 0.0003 inverse Å. The compounds were held in thin-walled (10 μm thick) glass capillaries with a diameter of 0.7 mm.

4. Results

The transition temperatures and the associated enthalpy changes are summarized in table 1. The B_2 phase appears on cooling from the isotropic phase in all the studied compounds except for **iWBVI**. This phase is followed by the B_7 phase at lower temperatures. The B_2–B_7 phase transition is accompanied by a very low enthalpy change. The **iWBVI** compound exhibits only one mesophase. The justification for the identification of phases is given later.

Characteristic features of phase transitions are seen in the DSC plots (see figure 1 for selected compounds (*a*) **8WBVI** and (*b*) **8WDVI**). The shape of the crystallization peak indicates gradual solidification. Comparison of the sum of enthalpies associated with the phase transitions on cooling and heating indicates

Table 1. Melting points, transition temperatures and transition enthalpies (in brackets) taken on cooling from the isotropic phase. R_n indicates the alkyl or alkoxy chain (see scheme 1).

Compound	R	m.p. °C (J g^{-1})	°C (J g^{-1})	B_7	°C (J g^{-1})	B_2	°C (J g^{-1})	I
5WBVI	$C_5H_{11}O$-	174 (+24.2)	156 (−16.8)	•	180 (−0.1)	•	204 (−13.1)	•
iWBVI	$CH_3CH(CH_3)CH_2CH_2O$-	183 (+13.1)	168 (−35.5)	•	191 (−19.5)	—		•
8WBVI	$C_8H_{17}O$-	162 (+26.0)	124 (−14.9)	•	196 (−1.3)	•	209 (−20.2)	•
10WBVI	$C_{10}H_{21}O$-	165 (+22.6)	112 (−11.9)	•	173 (−0.7)	•	213 (−22.2)	•
8WDVI	C_8H_{17}-	163 (+33.4)	118 (−5.2)	•	146 (−2.7)	•	195 (−24.1)	•
10WDVI	$C_{10}H_{21}$-	156 (+21.6)	126 (−18.1)	•	144 (−0.2)	•	200 (−29.4)	•

the existence of another phase transition in the solid phase at low temperatures. In some cases a partial recrystallization process occurs on heating which appears as a negative peak.

4.1. *Phase identification*

The high temperature phase observed for all materials except **iWBVI** exhibits a fan-shaped texture, typical for the B_2 phase. Usually stripes appear parallel to the smectic layers on cooling from the isotropic phase, see figure 2 (*a*) for **10WDVI**. The regions of the sample with stripes parallel to the direction of the light polarization of the crossed polarizers are in optical extinction, figure 2 (*a*). The extinction remains the same under a d.c. electric field of 0.5–1 V µm^{-1}, when the majority of the stripes have disappeared. Using an optical compensator we found that the long axis of the optical indicatrix is parallel to the smectic layer normal. The

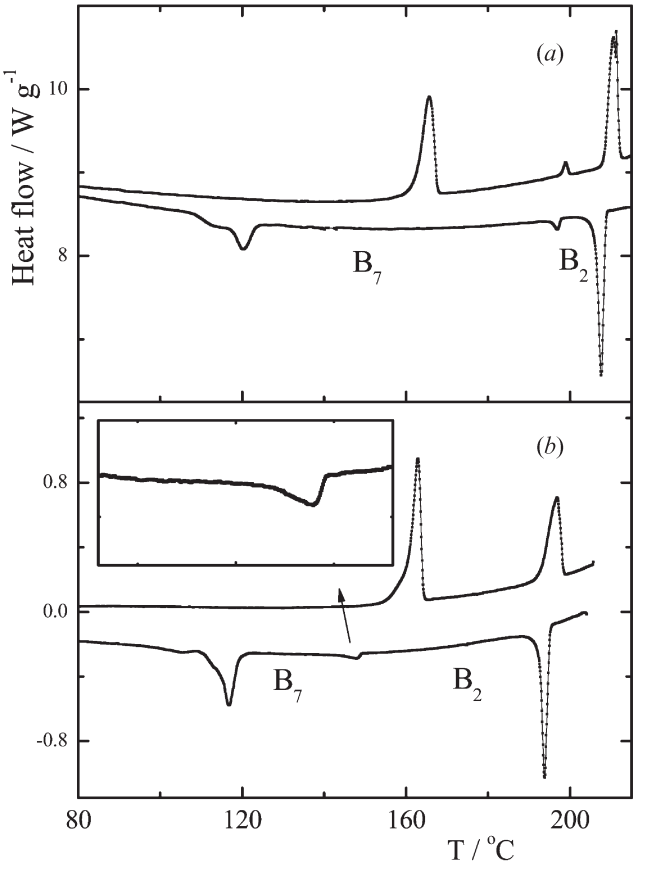

Figure 1. Thermograms for (*a*) **8WBVI**, and (*b*) **8WDVI**. Upper and lower curves show second heating and subsequent cooling runs, respectively. The inset in (*b*) shows the B_2–B_7 phase transition on a magnified scale.

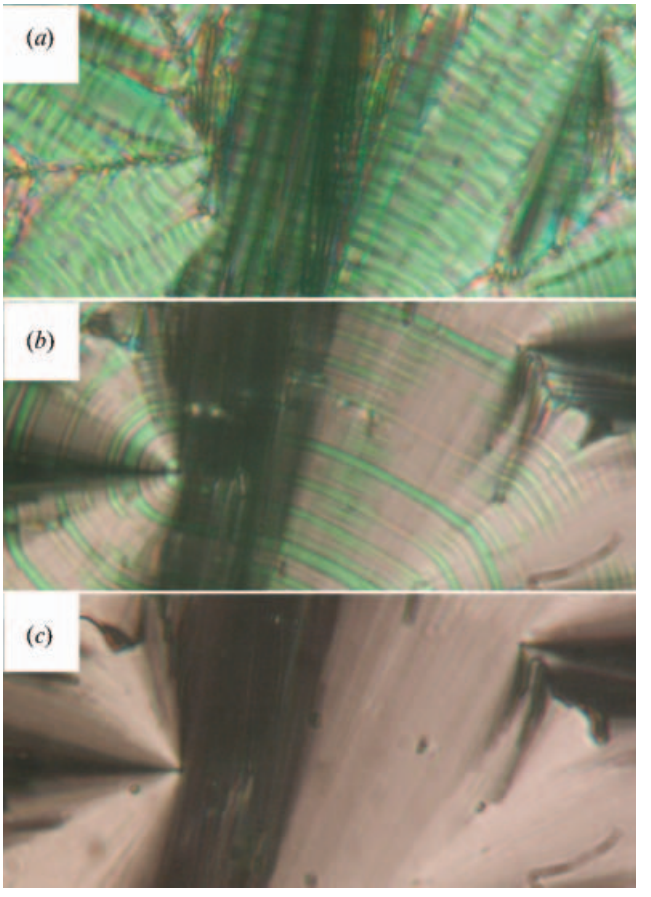

Figure 2. Texture of the B_2 phase for **10WDVI** at T=190°C (*a*) without field, (*b*) in a d.c. electric field of 10 V µm^{-1} and (*c*) 25 V µm^{-1}. Thickness of the sample was 6 µm; the width of the microphotograph represents 300 µm approx.

extinction position does not deviate from the previous optical axis even under high electric fields, figure 2 (*c*), when another field induced transition arises connected with a change of birefringence, c.f. figure 2 (*b*).

On very slow cooling from the isotropic phase large domains could be obtained instead of narrow stripes, see figure 3 (*a*) for **8WDVI**. Using monochromatic light we could distinguish the different behaviour of domains when de-crossing the analyser. The first type of domain, violet colour in figure 3 (*a*), has normal optical properties, i.e. four extinction brushes for crossed polarizer and analyser. The birefringence, Δn, measured by a calibrated Babinet–Soleil compensator, has been evaluated within 0.16 and 0.30 for the materials studied (0.16 for **8WDVI**). The second type of domain, green colour in figure 3 (*a*), exhibits extinction at parallel polarizers, which corresponds to the rotation of the polarized light plane by 90°. This angle is conserved regardless of sample thickness.

The applyication of a d.c. electric field of about $0.5\,V\,\mu m^{-1}$ causes the second type of domain to disappear and the sample becomes almost homogeneously coloured, violet fans for **8WDVI** in figure 3 (*b*). On increasing the value of the applied d.c. field (up to $5–10\,V\,\mu m^{-1}$ depending on material) we reach another field-induced transition; see figure 3 (*c*) where green domains corresponding to the high field structure have grown. Finally, fans with even higher birefringence have been observed; $\Delta n = 0.20$ for green domains in figure 3 (*d*).

The planar texture of the B_7 phase exhibits additional defects and deformation of the original fans. Only in the case of **iWBVI** does the B_7 phase appear just below the isotropic phase in the form of typical spiral and wire-like nuclei and elliptical domains.

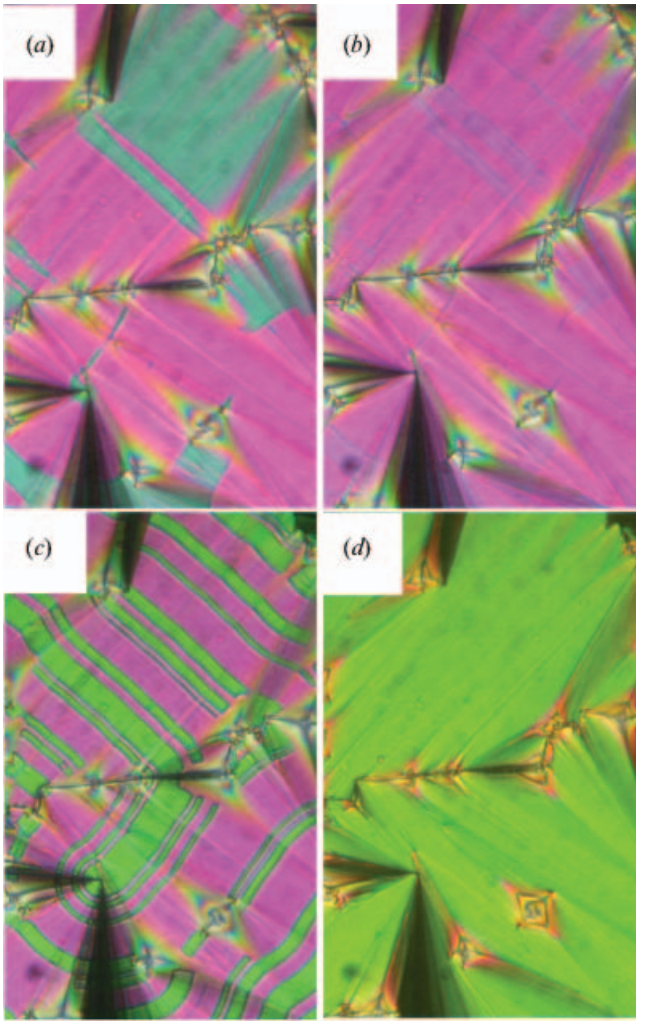

Figure 3. Planar sample textures of **8WDVI** in the B_2 phase at $T = 178°C$: (*a*) very slowly cooled from the isotropic phase without field; (*b*) with d.c. electric field $2\,V\,\mu m^{-1}$, (*c*) $12\,V\,\mu m^{-1}$, (*d*) $15\,V\,\mu m^{-1}$. The width of microphotographs represents 150 μm approx.

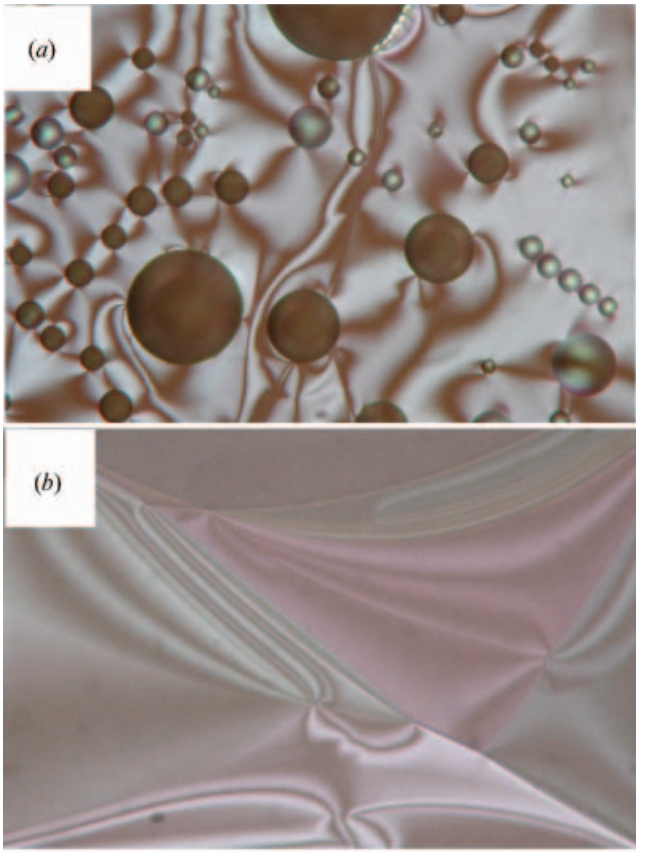

Figure 4. Textures of free-standing films: (a) phase transition from the isotropic to the B_2 phase of **10WDVI**; (*b*) the B_2 phase of **8WBVI** at 200°C. The widths of microphotographs are 150 μm.

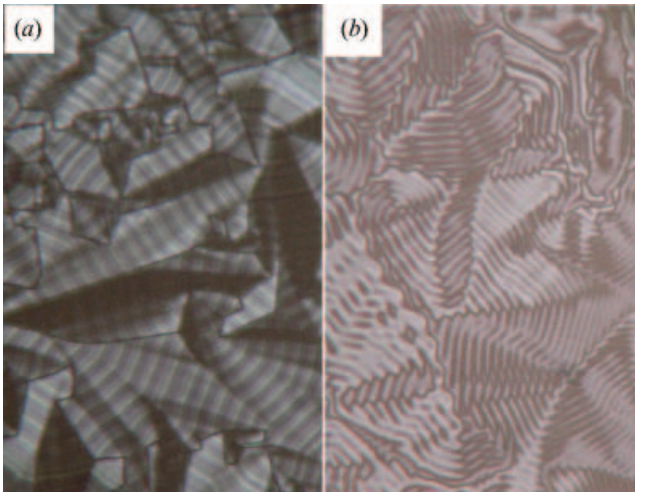

Figure 5. Free standing films in the B_7 phase for (*a*) **8WBVI** and (*b*) **8WDVI**. The widths of microphotographs are 150 µm.

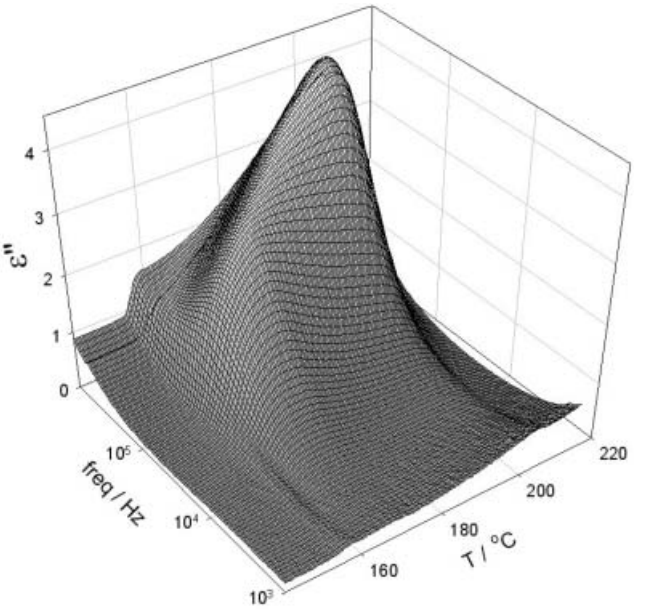

Figure 6. Temperature–frequency plots of the imaginary part of the dielectric permittivity taken on cooling for **8WDVI**.

Free-standing films have been succesfully prepared and studied for all the compounds. In figure 4 (*a*) the phase transition from the isotropic to the B_2 phase is shown with typical bubbles and defects which persist several degrees below the isotropic–B_2 phase transition. In figure 4 (*b*) the schlieren texture of the B_2 phase is shown for **8WBVI**, which exhibits a degeneracy of the director in-plane orientation.The texture in the B_7 phase exhibits regular stripe patterns; figures 5 (*a*) and 5 (*b*) for **8WBVI** and **8WDVI**, respectively. A similar texture has been observed in free-standing films of **iWBVI**, in which the B_7 phase is reached on cooling directly from the isotropic phase.

4.2. *Dielectric spectroscopy*

In the dielectric spectroscopy measurements, a weak single relaxation process was observed in the B_2 phase, which is quenched in the isotropic phase (see figure 6).When approaching the B_7 phase this mode starts to weaken, but it may still be visible a few degrees below the B_2–B_7 phase transition (see figure 7 for **8WDVI**). Fitting the dielectric data to the Cole–Cole formula, we obtain temperature dependences of dielectric strength, $\Delta\varepsilon(T)$, and relaxation frequency, $f_r(T)$. Two typical temperature dependences of $\Delta\varepsilon(T)$ and $f_r(T)$ are shown in figure 8. On cooling, $\Delta\varepsilon$ exhibits either a continuous steep decrease, figure 8 (*a*), or a jump down, figure 8 (*b*), at the phase transition to the B_7 phase. In the former case f_r exhibits an anomalous increase at this transition. In the B_7 phase $\Delta\varepsilon$ and f_r continues to decrease, but in many cases the mode is not visible in the B_7 phase. The low values of $\Delta\varepsilon$ and high f_r support the antiferroelectric character of the B_2 phase.

Antiferroelectric switching has been observed under a triangular wave field of 15 $V_{pp}\,\mu m^{-1}$, 20 Hz. Two distinct peaks in the polarization reversal current are clearly seen in the B_2 phase (see figure 9 for **8WDVI**). The spontaneous polarization $\mathbf{P}_s$ evaluated from the current, varies from 150 $nC\,cm^{-2}$ (**10WBVI**) to 400 $nC\,cm^{-2}$ (**8WDVI**). In the B_7 phase the electro-optic response was observed only near the B_2–B_7 phase transition.

4.3. *X-ray studies*

The X-ray pattern exhibits sharp small angle reflections and a diffuse scattering maximum in the large angle region (figure 10). This indicates a layered structure

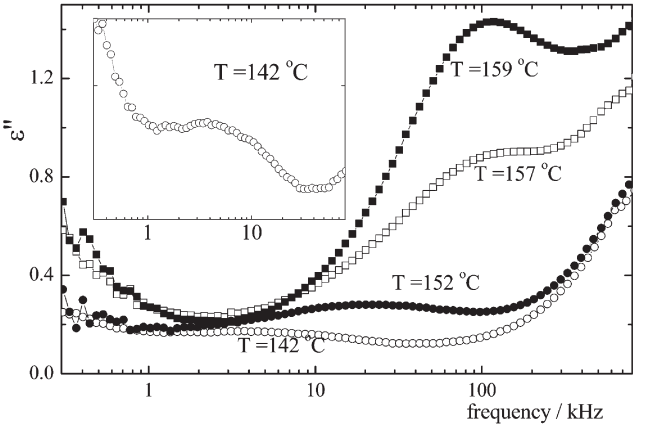

Figure 7. Frequency dependences of the imaginary part of the dielectric permittivity taken on cooling in the vicinity of the B_2–B_7 phase transition at 146°C for **8WDVI**.

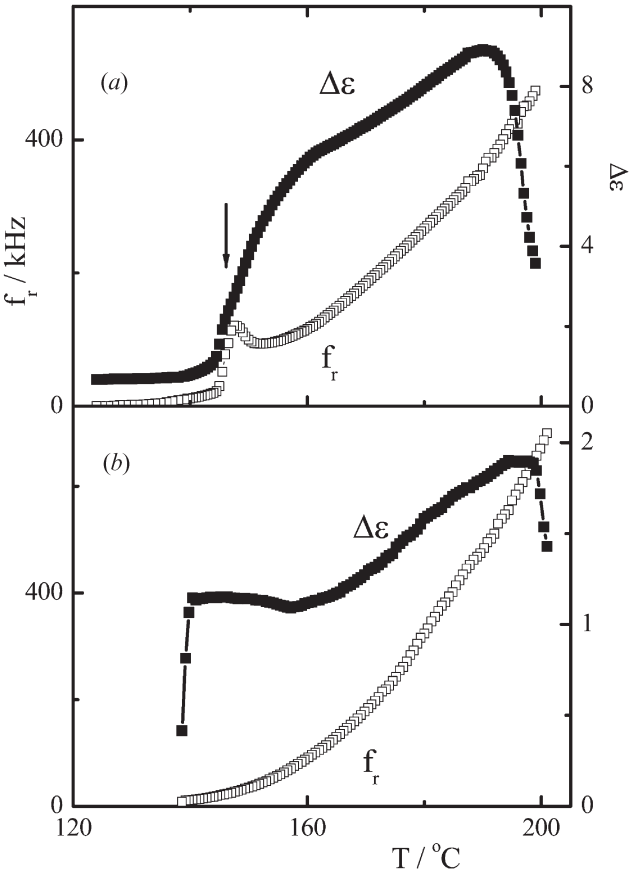

Figure 8. Fitted values of $\Delta\varepsilon$ and f_r for (a) **8WDVI** and (b) **10WDVI**.

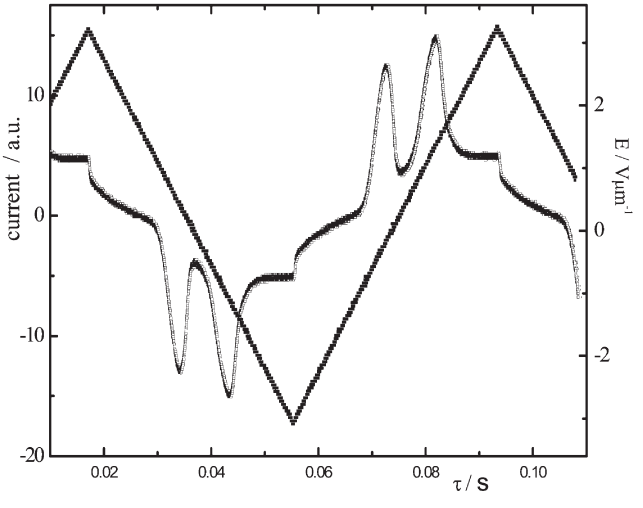

Figure 9. The switching current taken at 10 Hz and corresponding electric field profile in the B_2 phase at $T=180^{\circ}$C for **8WDVI**.

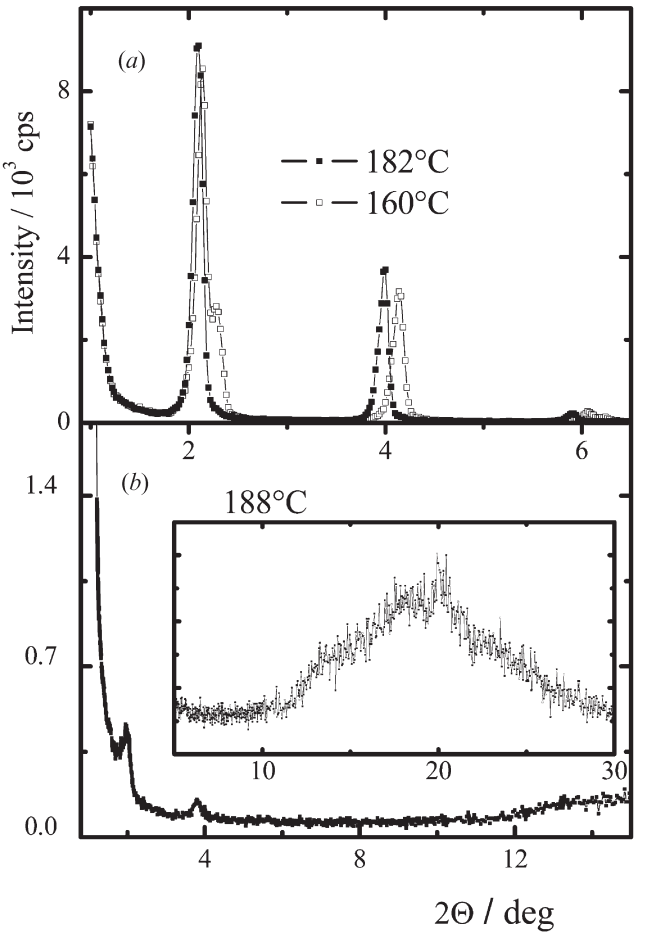

Figure 10. Small angle X-ray diagram of (*a*) **5WBVI** and (*b*) **8WDVI** at indicated temperatures. In the inset of (*b*) the wide angle region is enlarged.

with liquid-like molecular packing within the layers. The qualitative character of the X-ray data is very similar for both the B_2 and B_7 phases, see figure 10 (*a*). From the sharp inner reflections in the small angle region, which are present up to higher orders, the layer spacing d could be determined. The temperature dependence of d for **5WBVI** and **8WDVI** is shown in figures 11 (*a*) and 11 (*b*), respectively. While for **5WBVI** d does not change within the temperature range of the B_2 phase, for **8WDVI** d grows on cooling from the isotropic to the B_7 phase. For all compounds studied we found the layer spacing to be considerably smaller than the calculated molecular length l, which suggests a tilted arrangement of the molecules. The l values were found for every type of molecule assuming that the opening angle of the molecular arms is 120°. From the relationship $\cos\Theta=d/l$ the tilt angle could be determined as $\Theta=27^{\circ}$–29°.

To obtain more information on the structure of the low temperature phase, synchrotron studies have been

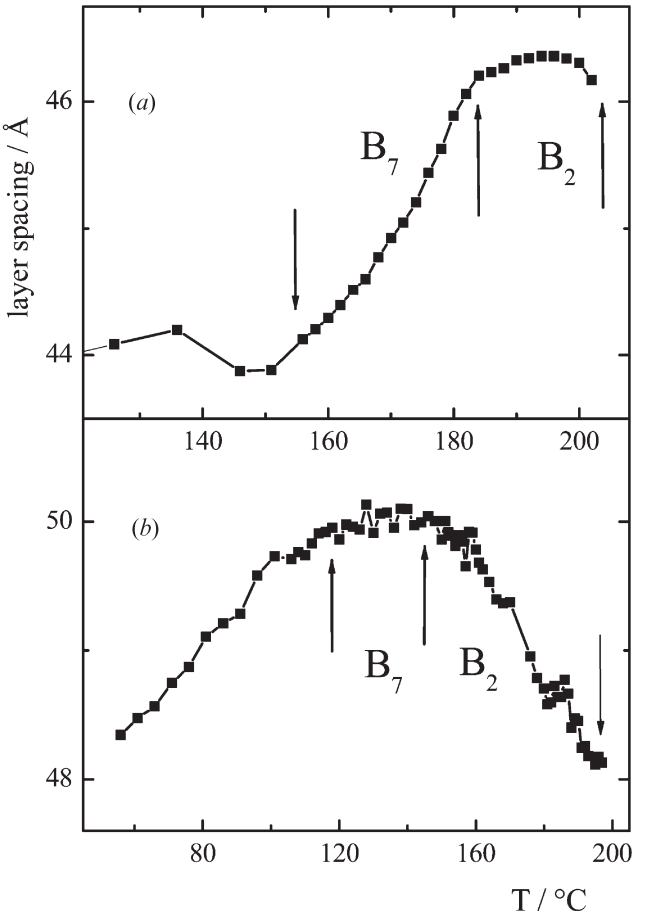

Figure 11. Temperature dependence of layer spacing for (*a*) **5WBVI** and (b) **8WDVI**.

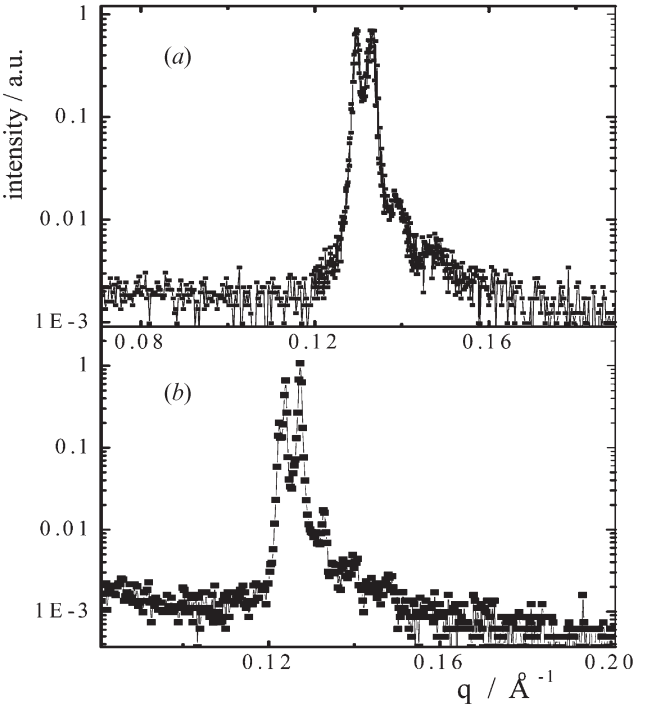

Figure 12. Synchrotron spectra measured in the B_7 phase for (*a*) **8WBVI** at $T=158^{\circ}C$ and (*b*) **10WBVI** at $T=168^{\circ}C$.

performed for **8WBVI** and **10WBVI**. The profile of the synchrotron data is presented in figures 12 (*a*) and 12 (*b*) for **8WBVI** and **10WBVI**, respectively. The powder scattering pattern for material **8WBVI** was indexed to a two-dimensional oblique lattice with lattice vectors of $q_s=0.1298\,\text{Å}^{-1}$ and $q_m=0.0199\,\text{Å}^{-1}$ with an opening angle of $\gamma=83.2^{\circ}$. The scattering pattern for material **10WBVI** was indexed to a similar lattice ($q_s=0.12388$, $q_m=0.01637\,\text{Å}^{-1}$, and $\gamma=81.2^{\circ}$). Both materials have form factors qualitatively identical to that of the first reported B_7 compound [20] allowing us to identify these phases as the B_7 phase.

5. Conclusions and discussion

We have synthesized thermally stable banana-type materials with one or two mesophases. Except for **iWBVI**, the B_2 phase appears below the isotropic phase on cooling. X-ray studies confirmed the layer character and provided information about layer spacing. From a comparison of the calculated values of molecular length with these values, the tilt angle has been determined as 27°–29°. The switching current, with two peaks and low $\Delta\varepsilon$ values, confirms the antiferroelectricity of the observed B_2 phase.

The texture observation in both planar samples and free-standing films are compatible with the B_2 phase structure. The observation of planar samples revealed a striped texture. On very slow cooling large domains appear instead of stripes. The domains that rotate the plane of polarized light disappear under a critical electric field, $\mathbf{E}_1$. At a field $\mathbf{E}_2>\mathbf{E}_1$ switching to the saturated ferroelectric structure takes place. The rotation of the plane of polarized light indicates a non-homogeneous (twisted) in-plane structure. We suppose that the molecular twist is imposed by surfaces. This structure and its behaviour in the electric field will be the subject of further studies.

In all the materials the non-twisted domains exhibit optical extinction when one of the crossed polarizers is parallel to the layer normal, which remains true for both zero field and high field states. Three models could satisfy such an observation. According to the model described in [2], the field-free structure would be the chiral structure (SmC_AP_A), while under the high electric field the racemic structure (SmC_AP_F) occurs. This model should be disregarded as it involves the same birefringence in both field and field-free structures in

contrast to the experimental results. Besides, it supposes reversible change of chirality during field switching. A second model suggests that both high and zero field states are composed of chiral mesoscopic grains of opposite handedness [21]. Under the field, the SmC_AP_A structure in each grain is changed to SmC_SP_F, the molecules being inclined to the opposite directions in adjacent grains. A third model has been proposed, comprising racemic SmC_SP_A domains with the opposite inclination of molecules, which are separated by boundaries parallel to the smectic layers [22]. These domains could be observed as a regular stripe pattern, see figure 2 (*a*), or if very narrow they are not visible and we observe homogeneous colour. Under the field the structure changes to racemic SmC_AP_F, which may be accompanied by the disappearance of the stripes. In models 2 and 3 the change of birefringence during switching can be envisaged. Moreover model 3 can also explain the stripe structure figure 2 (*a*).

The low temperature phase is attributed to the B_7 phase. The in-plane modulations observed in free-standing films in this phase for all the compounds studied are characteristic feature of the B_7 phase. Synchrotron studies confirmed that it is the same variant as previously described [20] and may differ from that reported for other compounds [7, 23]. The existence of two variants of the B_7 phase has already been mentioned [23].

Acknowledgements

This work was supported by Research Project of the Academy of Sciences of the Czech Republic No. AVOZ10100520.

References

[1] T. Niori, T. Sekine, J. Watanabe, T. Furukawa, H. Takezoe. *J. mater. Chem.*, **6**, 1231 (1996).
[2] D.M. Walba, E. Körblova, R. Shao, J.E. Maclennan, D.R. Link, M.A. Glaser, N.A. Clark. *Science*, **288**, 2181 (2000).
[3] J. Thisayukta, Y. Nakayama, J. Watanabe. *Liq. Cryst.*, **27**, 1129 (2000).
[4] M. Hird, J.W. Goodby, N. Gough, K.J. Toyne. *J. mater. Chem.*, **11**, 2732 (2001).
[5] C.V. Yelamaggad, U.S. Hiremath, A. Nagamani, D.S. Shankar Rao, S. Krishna Prasad. *J. mater. Chem.*, **11**, 1818 (2001).
[6] D.M. Walba, E. Körblova, R. Shao, N.A. Clark. *J. mater. Chem.*, **11**, 2743 (2001).
[7] D.A. Coleman, J. Fernsler, N. Chattham, M. Nakata, Y. Takanishi, E. Körblova, D.R. Link, R.-F. Shao, W.G. Jang, J.E. Maclennan, O. Mondain-Monval, C. Boyer, W. Weissflog, G. Pelzl, L.-C. Chien, J. Zasadzinski, J. Watanabe, D.M. Walba, H. Takezoe, N.A. Clark. *Science*, **301**, 1204 (2003).
[8] G. Pelzl, S. Diele, W. Weissflog. *Adv. Mater.*, **11**, 707 (1999).
[9] I. Wirth, S. Diele, A. Eremin, G. Pelzl, S. Grande, L. Kovalenko, N. Pancenko, W. Weissflog. *J. mater. Chem.*, **11**, 1642 (2001).
[10] H. Nádasi, W. Weissflog, A. Eremin, G. Pelzl, S. Diele, B. Das, S. Grande. *J. mater. Chem.*, **12**, 1316 (2002).
[11] J. Mieczkowski, K. Gomola, J. Koseska, D. Pociecha, J. Szydlowska, E. Gorecka. *J. mater. Chem.*, **13**, 2132 (2003).
[12] R. Amarantha Reddy, B.K. Sadashiva. *J. mater. Chem.*, **14**, 1936 (2004).
[13] H.N. Shreenivasa Murthy, B.K. Sadashiva. *Liq. Cryst.*, **30**, 1051 (2003).
[14] V. Prasad, S.-W. Kang, S. Kumar. *J. mater. Chem.*, **13**, 1259 (2003).
[15] H.N. Shreenivasa Murthy, B.K. Sadashiva. *J. mater. Chem.*, **13**, 2863 (2003).
[16] R. Amarantha Reddy, B.K. Sadashiva. *Liq. Cryst.*, **30**, 1031 (2003).
[17] W. Weissflog, H. Nádasi, U. Dunemann, G. Pelzl, S. Diele, A. Eremin, H. Kresse. *J. mater. Chem.*, **11**, 2748 (2001).
[18] A. Eremin, H. Nádasi, G. Pelzl, S. Diele, H. Kresse, W. Weissflog, S. Grande. *Phys. Chem. chem. Phys.*, **6**, 1290 (2004).
[19] M. Kašpar, V. Hamplová, V. Novotná, M. Glogarová, P. Vaněk. *J. mater. Chem.*, **12**, 2221 (2002).
[20] G. Pelzl, S. Diele, A. Jakli, Ch. Lischka, I. Wirth, W. Weissflog. *Liq. Cryst.*, **26**, 135 (1999).
[21] C.L. Folcia, J. Ortega, J. Etxebarria. *Liq. Cryst.*, **30**, 1189 (2003).
[22] P. Pyc, J. Mieczkowski, D. Pociecha, E. Gorecka, B. Donnio, D. Guillon. *J. mater. Chem.*, **14**, 2374 (2004).
[23] G. Pelzl, M.W. Schröder, U. Dunemann, S. Diele, W. Weissflog, C. Jones, D.A. Coleman, N.A. Clark, R. Stannarius, J. Li, B. Das, S. Grande. *J. mater. Chem.*, **14**, 2492 (2004).